Advanced AI computing enabled by 2D material-based neuromorphic devices

Check for updates

Yunseok Choi[1,10], Siwoo Jeong[2,10], Hyeonu Jeong[3,4,10], Sangmoon Han[1], Jonghyeon Ko[5,6], Si Eun Yu[3], Zhihao Xu[1,7], Min Seong Chae[8], Minjae Son[3], Yuan Meng[1], Shijue Xu[1,7], Ji-Hoon Kang[3,4] ✉, Sungchul Mun[5,8,9] ✉ & Sang-Hoon Bae[1,7] ✉

Neuromorphic systems are emerging as a promising alternative to revolutionize silicon-based computing devices. Two-dimensional materials are considered promising candidates for active materials due to their unique advantages. This review provides a comprehensive overview of neuromorphic computing based on 2D materials, encompassing the development from the synaptic devices based on 2D materials to the neuromorphic system demonstration. Besides, we further outline various applications of neuromorphic computing in the emerging applications of neuromorphic computing

Classical computing relying on Neumann architecture features sequential processing, where the separation of memory and logic units are interconnected via a bus structure[1–3]. This architecture, combined with the miniaturization of electronics predicted by Moore's Law, has enabled exponential growth in computational power over the past several decades[4,5]. However, the von Neumann bottleneck is manifesting over time, due to the increasing load of data transfer between memory and processing units, significantly hindering performance by consuming up to 60% of computing energy in this process and also limiting device integration density[6–9]. Moreover, the explosive growth of data exacerbates the imbalance between data volume and bus capacity. A phenomenon thus emerged as the "memory wall," which restricts the speed and efficiency of modern computing systems, especially in data-intensive applications such as artificial intelligence (AI), machine learning, and big data analytics[10,11].

Inspired by the human brain, neuromorphic computing has garnered significant attention for its excellent potential to mimic the brain's excellent energy efficiency and computational capability. Distinctive from conventional digital systems that rely on binary logic, neuromorphic systems utilize analog and event-driven processing through dynamic interactions of neurons and synapses, offering advantages in power efficiency and handling unstructured data. To this end, two-dimensional (2D) materials offer several unique characteristics that allow them to overcome the limitations encountered by traditional two-dimensional (3D) bulk materials in neuromorphic computing[12–14]. Thanks to their atomically thin thickness, 2D materials exhibit excellent electrical properties, such as high carrier mobility and low power consumption, which are crucial for reducing the power consumption of neuromorphic devices. Additionally, 2D materials serve as promising building blocks due to their excellent electronic properties, and high mechanical flexibility rising from thin thickness, enabling the van der Waals (vdW) stacking of different materials to form vdW heterojunctions that retain individual material properties while introducing new functionalities[13,15,16]. This atomically thin thickness also facilitates monolithic 3D integration (M3D) with great potential for high vertical integration density, enabling the development of densely packed, scalable neuromorphic circuits that can mimic the complex connectivity of biological neural networks[17]. Moreover, the excellent tunability of 2D materials also allows for more precise control over synaptic weights that are essential for the reliable and efficient emulation of short-term plasticity (STP) and long-term plasticity (LTP) in artificial neural networks (ANNs)[18,19]. These properties collectively enable 2D materials to address the challenges of scalability, power efficiency, analog computation, and synaptic plasticity that hinder conventional neuromorphic systems.

Here, we catalog the device architectures that have been proposed and realized using 2D materials from 2D to 3D memory devices as well as their advanced configurations. System-level implications of integrated 2D materials into neuromorphic circuits have also been discussed with the advanced approaches that can enhance the performance and efficiency of neuromorphic computing. Moreover, we review the potential applications

[1]Department of Mechanical Engineering and Materials Science, Washington University in St. Louis, St. Louis, USA. [2]Department of Sports Rehabilitation Medicine, Kyungil University, Gyeongsan, South Korea. [3]Department of Electrical and Computer Engineering, Inha University, Incheon, South Korea. [4]Program in Semiconductor Convergence, Inha University, Incheon, South Korea. [5]Convergence Institute of Human Data Technology, Jeonju University, Jeonju, South Korea. [6]School of Information Systems, Queensland University of Technology, Brisbane, Australia. [7]The Institution of Materials Science and Engineering, Washington University in St. Louis, Saint Louis, USA. [8]Department of Industrial Engineering, Jeonju University, Jeonju, South Korea. [9]Department of Data Engineering, Jeonju University, Jeonju, South Korea. [10]These authors contributed equally: Yunseok Choi, Siwoo Jeong, Hyeonu Jeong. ✉e-mail: jhkang57@inha.ac.kr; sungchul.mun@jj.ac.kr; sbae22@wustl.edu

of the neuromorphic systems connected with various industries. Practical challenges, emerging opportunities, and perspectives for the advanced 2D neuromorphic computing system are outlined as well in the conclusion section.

Synaptic devices based on 2D materials

Neuromorphic synaptic devices are capable of retaining their electrical state after being deactivated, and the ones composed of 2D materials have emerged as a promising area of research. The devices can be generally categorized into two types: two-terminal (2 T) memory device and three-terminal (3 T) memory device, where 2D materials are predominantly utilized as dielectric or working layers in 2 T device and dielectric or channel layers in 3 T device. Additionally, hybrid structures of 2 T and 3 T synaptic devices and multi-terminal devices have been developed to enhance memory device functionalities[20–22]. Memristors using 2D materials are commonly arranged in a cross-bar array structure[23] and are categorized into four configurations: 1 memristor (1 M)[24], 1 diode 1 memristor (1D1M)[25], 1 selector 1 memristor (1S1M)[26], and 1 transistor 1 memristor (1T1M)[17]. Each configuration exhibits unique characteristics that improve current directionality and overall memristor functionality.

2 T synaptic memristor has a simple structure consisting mainly of two conductive electrodes and an active layer material in between. The active layer-based 2D material enables the construction of large crossbar arrays with low energy consumption and space. The fundamental concept of a memristor is based on switching the device between two different states: a high resistance or low polarized state (HRS) and a low resistance or high polarized state (LRS)[27]. In a resistive memory, the process of moving from HRS to LRS close to the conductor is known as a 'SET' operation, while the reverse process is known as a 'RESET' operation. These states can be represented as binary values of '0' and '1', where the low resistance state (on state) and the high resistance state (off state). Leveraging this mechanism,

various synaptic functions can be emulated, including excitatory post-synaptic current (EPSC), spike-timing-dependent plasticity (STDP), paired-pulse facilitation (PPF), and spike rate-dependent plasticity (SRDP)[28].

Resistive switching memory (RSM) (2 T) devices are promising synaptic devices with fast switching speed and scalability. The electrode materials for RSM typically consist of either active metal materials (such as Ag and Cu), which participate in the formation of conductive filaments, or inert metal materials (like Au and Pt) serving as stable counter electrodes[29,30]. Additionally, various transition metal dichalcogenide (TMD) semiconductor materials, including h-BN, MoS_2, WS_2, WSe_2, and $MoSe_2$, have been demonstrated as active layer materials that can enhance switching performance and mitigate device degradation even under repetitive stress[31]. There are two primary mechanisms for resistive switching based on the formation of conductive filaments: electrochemical metallization (ECM), and valence change mechanism (VCM). ECM devices consist of a dielectric layer positioned between an upper electrode made of an active metal and a lower electrode made from an inert metal for ion migration for the formation and dissolution of metal filaments[32,33]. VCM devices have electrodes made from inert metals and the dielectric layer is a TMD[34,35]. When a voltage is applied to the electrodes, an electric field is generated, which induces reversible oxidation and reduction reactions, leading to the formation of conductive filaments. For instance, a novel multilevel electronic synaptic device was proposed based on a MoS_2 memristor array (Fig. 1a, b)[36]. The device utilizes a 4×4 crossbar architecture with a highly crystalline MoS_2 film. The thin MoS_2 layer (~ 2.1 nm) enables low voltage switching and demonstrates excellent memory performance with an endurance of over 500 sweep cycles and a retention time of approximately 10^4 s (Fig. 1c, d). The proposed MoS_2 memristor array achieves high recognition accuracy in deep neural network (DNN), with an accuracy of 98.55% (Fig. 1e).
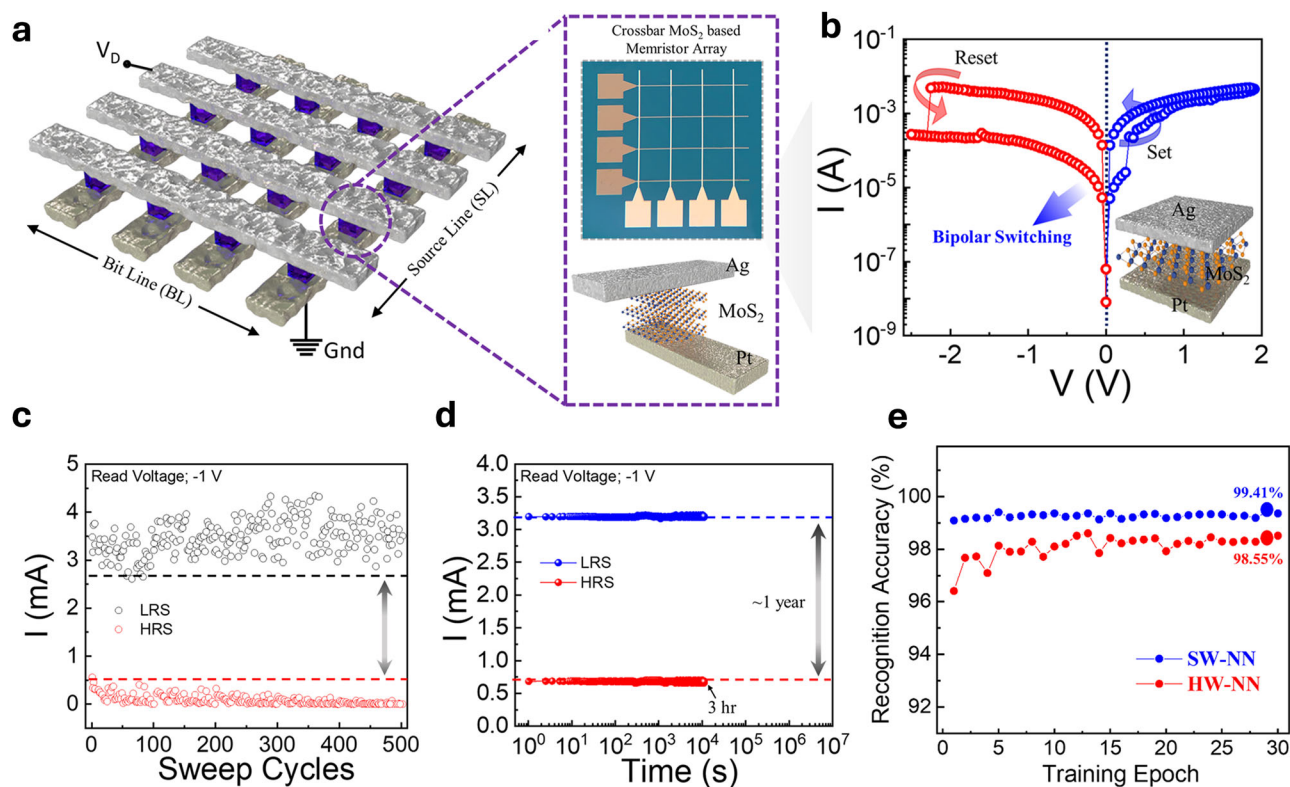
Fig. 1 | Multilevel electronic synaptic device based on a MoS_2 memristor array. a Architectural schematic layout of the proposed 4×4 crossbar memristor array based on large-area direct grown MoS_2 with 3D section view of the single memristor[36]. **b** Bipolar memory switching curve of the MoS_2 memristor devices under voltages between -2.5 V and 2 V. **c** Memory operations of proposed memristor device in terms of endurance up to 500 sweep cycles at a read voltage of -1 V and **d** retention, measured up to 10^4 s at a read voltage of -1 V. **e** Recognition accuracy graph of SW-NN and HW-NN for each training epoch.
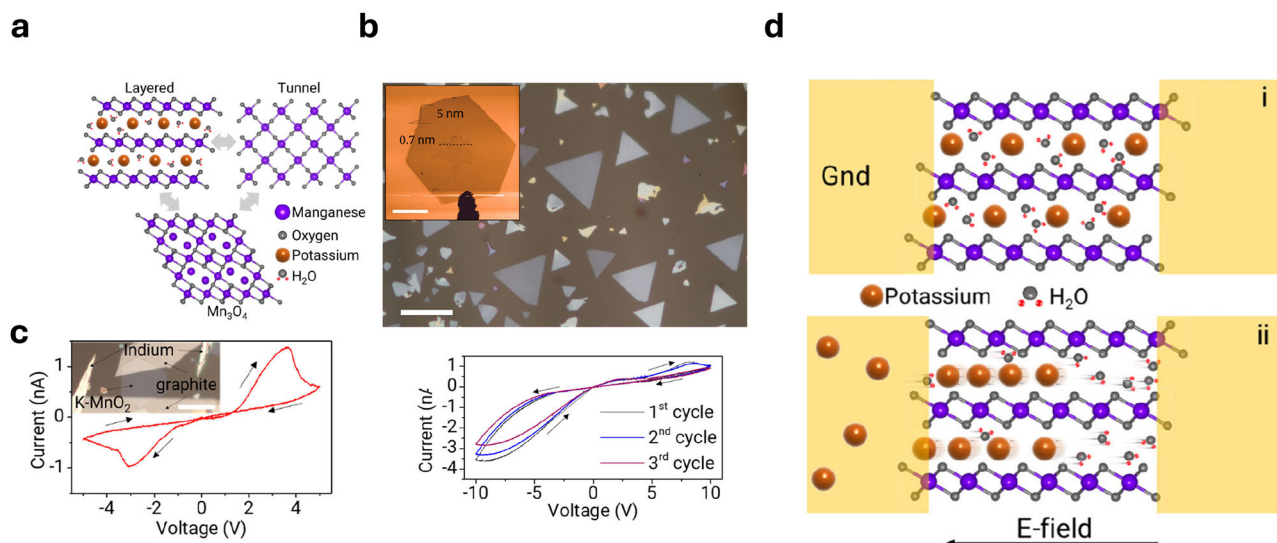
Fig. 2 | Electric field-driven reversible phase transitions in two-dimensional (2D) materials. a Representative schematic of layered and tunnel polymorphs of MnO_2 and, Mn_3O_4. **b** Optical microscope image of 2D K-MnO_2 crystals on a sapphire substrate[37]. **c** I–V cycle from a graphite/K-MnO_2/graphite memristive device. **d** Schematics depict the condition when panel i with no bias is applied and panel ii when bias is applied.

Phase change memory (PCM) (2 T) is a non-volatile memory (NVM) technology utilizing the reversible phase change properties of materials to store data by applying electrical pulses. Compared to bulk PCM, 2D materials are more sensitive to external stimuli thanks to their atomic-level thickness. As a result, phase transitions in 2D materials can be easily induced by various external stimuli such as strain, ion insertion, or electrostatic doping[37]. Unlike conventional phase change materials that switch between amorphous and crystalline states, TMDs with various polymorphs exhibit structural phase transitions. In particular, MoS_2 undergoes a phase transition between a hexagonal structure (2H phase) and a distorted octahedral structure (1 T or 1 T′ phase)[21,35]. Furthermore, Electric-field-induced reversible phase transitions in 2D potassium-intercalated manganese dioxide are proposed (K-MnO_2)[37]. These crystals were as thin as 5 nm with atomic layer thicknesses of 0.7 nm, and potassium ions spontaneously intercalated into the MnO_2 structure during synthesis, contributing to ionic conduction (Fig. 2a, b). Under moderate bias conditions of around 10 V, distinct phase transitions were observed, where the material switched between a layered and spinel structure (Fig. 2c–e). The voltage decay time constant (λ) for devices was found to be 81 ± 10 s/μm^2 and the devices maintained their performance over more than 5,600 cycles of potentiation and depression.

A typical 3 T transistor device consists of a structure that includes electrodes, a dielectric layer, and a channel layer. The gate electrode serves as the presynaptic node, while the source and drain electrodes act as the postsynaptic nodes. Distinctive from 2 T memristors, 3 T transistors feature a gate terminal, which allows for the modulation of channel conductance via dynamic resistive switching, thereby enabling multi-level data storage. Superior synaptic weight updates can be achieved through multi-gate modulation, making the device suitable for learning in neuromorphic computing systems. Additionally, transistor-based structures are capable of minimizing sneak currents, reducing power consumption, supporting analog computing, and enabling massively parallel processing[38].

First, synapse-mimicking devices in floating-gate memory or charge trapping-based memory structures typically consist of a sandwich structure for memory including a tunnel oxide insulating layer, a charge trapping layer, and a control gate[39]. The charge trapping layer is inserted between the gate and channel regions to store charge[40]. The advantage of this device lies in its technical maturity, inherited from transitional transistors, and the presence of a tunneling layer ensures long-term data retention without charge loss. The mechanism works by applying a voltage to the control gate that creates an electric field allowing electrons to tunnel into the charge

trapping layer[41]. Once the electrons tunnel, they become trapped in this layer, which is typically engineered with traps or defects that can store electrons for extended periods. Heterojunctions of 2D materials act as carrier traps, as the energy band alignment of the heterojunction and defects in the material coexist to modulate the conductivity of the channel. An ultrafast bipolar flash memory was proposed based on 2D semiconductor materials, enabling self-activated in-memory computing[42]. The key structure consists of layers of Al_2O_3, HfO_2, h-BN, and WSe_2, serving as the blocking oxide, charge-trapping layer, tunneling barrier, and semiconductor channel, respectively (Fig. 3a). When a gate voltage is applied, electrons tunnel into the HfO_2 layer and are stored there, turning the channel into n-type. Once charges are trapped in the HfO_2 layer, they modulate the Fermi level of the WSe_2 channel, determining whether the channel behaves as an n-type or p-type (Fig. 3b). The programming speed of the bipolar flash memory is around $20 \sim 30$ ns, which is three times faster than that of conventional flash memory (Fig. 3c). Besides, it also demonstrates an endurance of over 8 million cycles, consuming only 5 fJ of energy per MAC operation, showcasing extremely low power consumption (Fig. 3d).

Electrolyte-layer-based synaptic devices use electrolytes as gate insulators. They can be broadly divided into two types: electrostatic modulation and electrochemical doping. In the case of electrostatic modulation, the semiconductor layer is composed of a material that is impermeable to the ions from the electrolyte layer. When a gate voltage is applied, the movement of ions is influenced, and the resulting electric field causes ions to accumulate at the interface between the semiconductor and electrolyte layers, forming an electric double layer (EDL) that modulates the conductivity state of the device[43,44]. In contrast, electrochemical methods also form an electric double layer, but the ions from the electrolyte layer can permeate into the semiconductor layer, resulting in further modulation of the channel conductance[45,46]. Electrolyte-layer-based synaptic devices exhibit advantages in linear and symmetric updates to the conductance states. However, since their operation relies on the physical movement of ions, they suffer from slower conductance state updates and are more vulnerable to thermal effects.

Ferroelectric field-effect transistors (Fe-FETs) are being developed by integrating insulators with ferroelectric properties into conventional thin-film transistor (TFT) structures[47]. Ferroelectric materials exhibit spontaneous polarization which used for memory function. Their high dielectric properties help to increase layer thickness to prevent current leakage and polarized layer should be carefully designed to accommodate various 2D/3D structures[48]. The direction of polarization in these materials can be controlled by an external electric field, which in turn affects their conductivity[49].
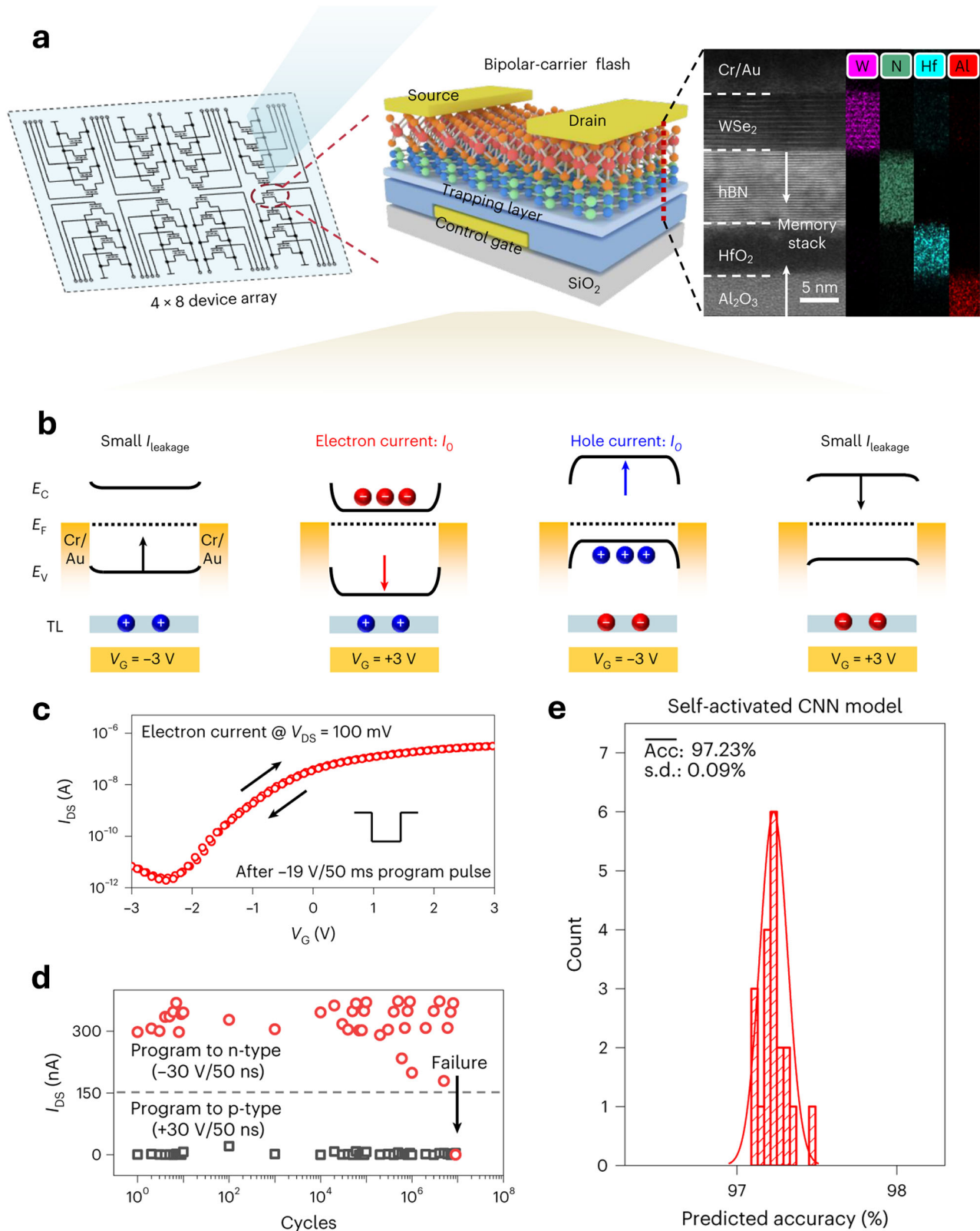
Fig. 3 | An ultrafast bipolar flash memory based on two-dimensional (2D) semiconductor materials. a Illustration of the bipolar flash array, containing 4×8 devices[42]. **b** Band diagrams of a device with different charges stored. Left: stored holes in the trapping layer after a negative pulse. Right: stored electrons in the trapping layer after a positive pulse. **c** The electron and hole current double-sweep transfer characteristic (I_{DS} versus V_G) of n-type (-19 V/50 ms programmed). **d** Device endurance test. **e** The test accuracy with self-activated CNN model.
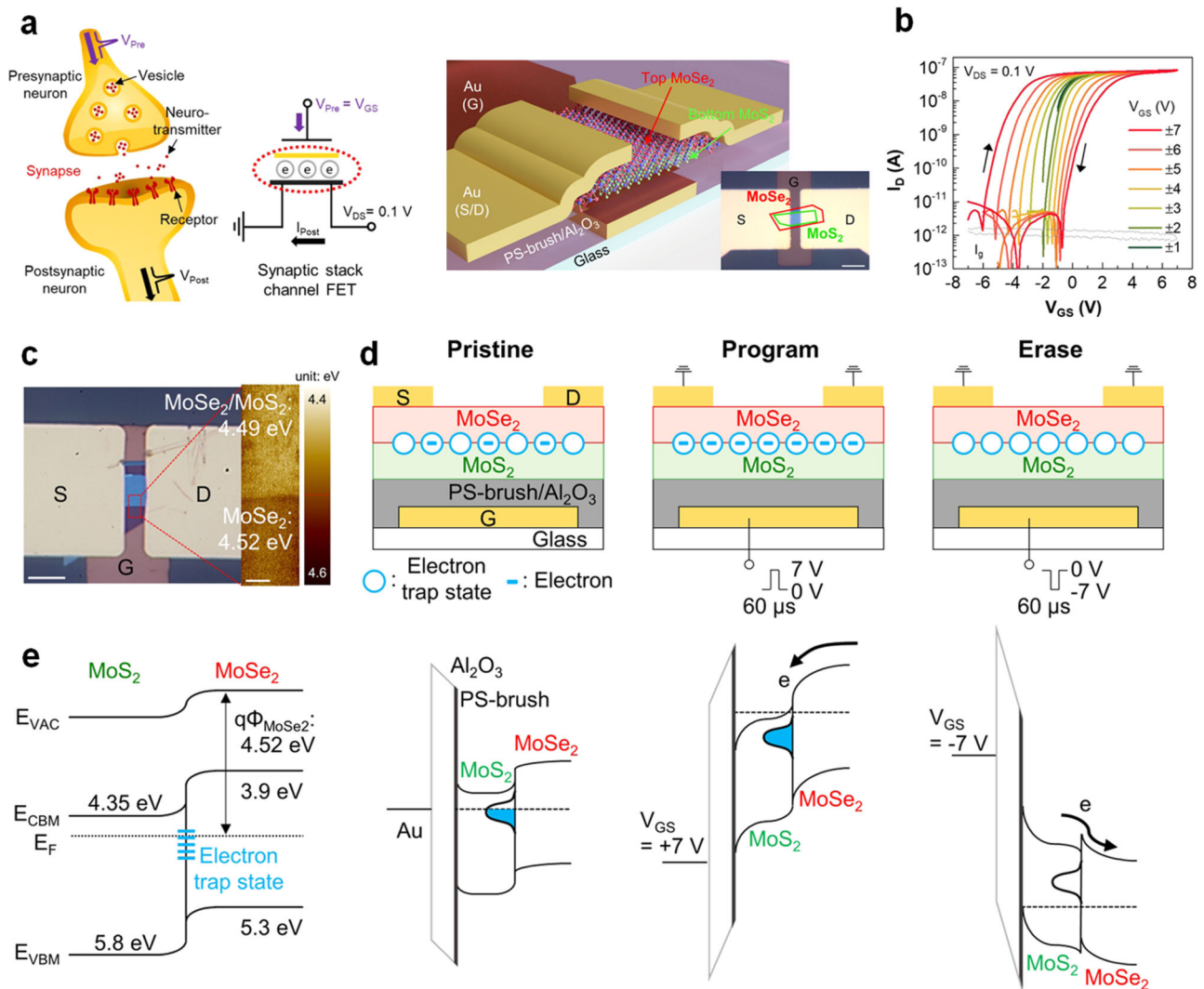
Fig. 4 | Ferroelectric gate using a bottom-gate MFMIS structure. a Schematic illustration of a biological synapse in a neuron system and our synaptic stack channel FET for neuromorphic function. **b** Transfer curves of $MoSe_2/MoS_2$ stack channel memory FET, showing asymmetric memory hysteresis behavior as measured under the double sweep of V_{GS}. **c** OM image of a $MoSe_2/MoS_2$ stack channel memory FET. **d** 2D schematic structures of our $MoSe_2/MoS_2$ stack channel FET to describe electron traps at the $MoSe_2/MoS_2$ heterojunction interface **e.** Band diagram of $MoSe_2/MoS_2$ heterojunction and analytical energy band diagrams of channel FET under corresponding **d**[84].

2D ferroelectric materials can serve as the channel material, offering potential improvements in device performance. Yeonsu Jeong et al. reported the development and application of $MoSe_2/MoS_2$ heterojunction-based FETs for multilevel memory, multiscale display, and synaptic functions[50]. The $MoSe_2/MoS_2$ heterojunction FETs are constructed using a bottom-gate metal-ferroelectric-metal-insulator-semiconductor (MFMIS) architecture (Fig. 4a, c). The device consists of a $MoSe_2/MoS_2$ heterojunction as the channel layer, a HfO_2 ferroelectric layer, and a metal gate electrode. This structure is designed to leverage the strong charge trapping capabilities and polarization properties of the HfO_2 layer, enabling precise control over the channel's conductance (Fig. 4d, e). The $MoSe_2/MoS_2$ FETs exhibit excellent electrical properties, such as a high on/off current ratio exceeding 10^7, robust endurance over 10^{12} cycles, and a minimal device-to-device variation of approximately 0.5% (Fig. 4b). Table 1 provides a summary of neuromorphic computing synaptic devices for comprehensive understanding.

Neuromorphic system demonstration
As memristors have been widely studied and proven to be promising as synaptic devices, research on neuromorphic systems has also accelerated. Biological neural networks involve two major phases: learning and inference. Neuromorphic systems aim to mimic these phases. To implement these functionalities in neuromorphic systems, it is essential to design systems capable of accurately storing weights and processing input/output operations. The implementation of neuromorphic systems requires three key components: synapses, neurons, and peripheral circuits.

1. **Synapses** are responsible for information storage and processing. They emulate the learning and memory functions of biological synapses by regulating the strength of signals (i.e., synaptic weights) transmitted between neurons. This can be realized using various emerging memory technologies such as memristors or memtransistors, which adjust their electrical properties dynamically based on prior signals, enabling the system to learn and adapt.
2. **Neurons** receive input from synapses, integrate these signals, and generate outputs based on the inputs. For instance, in systems that mimic spiking neural networks (SNNs), neurons accumulate input signals and generate spikes once a threshold is exceeded, emulating the behavior of biological neurons (e.g., Leaky integrate-and-fire (LIF) model). These processed signals are then transmitted to other neurons or synapses, facilitating communication across the network.
3. **Peripheral circuits** manage the interactions between neurons and synapses, facilitating learning and inference, and ensuring the smooth

Table 1 | Summary of 2 T and 3 T memory devices based on 2D materials

|	Memory Type	Device Structure	2D Material	On/Off Ratio	Operation Voltage (V)	Endurance (Cycle)	Retention(s)	Ref
2 T	ECM	Ag/MoS$_2$/Pt	MoS$_2$	10^3	0.8/−0.6	10^6	10^5	85
	ECM	Ag/Mxene/SiO$_2$/Pt	MXene	10^3	0.18/−1	100	10^4	86
	ECM	Ag/V$_2$C/TiO$_2$/W	Mxene (V$_2$C)	10^2	0.6/−0.2	40	10^3	87
	ECM	Ag/MoS$_2$	MoS$_2$	10^4	<1	300	0.1 s	88
	ECM	ITO/CdPS$_3$/Ag	CdPS$_3$	10^2	−0.93	100	-	89
	VCM	Ta/Ta$_2$O$_5$/AiN/G	Graphene	10	±4	10^4	-	90
	VCM	TiN/AlN/G/Pd	Graphene	10	0.16/−0.32	500	10^4	91
	VCM	Au/h-BN/Au	h-BN	10^5	0.75/−0.4	50	10^6	92
	PCM	rGO/FE-Mxene/rGO	rGO/FE-Mxene	10^3	−3.29/−1.65	10^3	4000	93
3 T	Charge Trapping Gate	(Cr/Au)/WSe$_2$/SiO$_2$/Si	WSe$_2$	10^3	30	100	600	41
	Floating Gate	(Cr/Au)/MoS$_2$/h-BN/Graphene	MoS$_2$/Graphene	10^4	±6	10^5	10^4	94
	Floating Gate	(Cr/Au)/WSe$_2$/ MoS$_2$, h-BN/ HfS$_2$/ Al$_2$O$_3$/Si	WSe$_2$/MoS$_2$, h-BN/HfS$_2$	10^3	±20	100	100	95
	EDLT	ITO/Mxene/Ag	Mxene (Ti$_2$C$_2$Tx)	10^3	+5/−2	50	20	96
	ECT	Graphene/LFP/PEO/Cu	Graphene	20	-	500	10^4	97
	FeFET	Au/Cr /α-In$_2$Se$_3$/Al$_2$O$_3$/Si	α-In$_2$Se$_3$	10^6	2	2000	10^4	98
	FeFET	Au/Pd /α-In$_2$Se$_3$/Pd/Au	α-In$_2$Se$_3$	10^3	2	300	-	99
	FeFET	Electrode/h-BN /α-In$_2$Se$_3$ /h-BN/Al$_2$O$_3$/Si	α-In$_2$Se$_3$	10^3	±8	500	500	100

operation of the implemented neuromorphic system. For inputs, it is necessary to amplify electrical signals obtained from sensors or artificially created inputs to provide sufficient voltage required for the fabricated neurons and synapses. Additional circuits such as feedback circuits and activation functions are also necessary to implement the operation of fabricated neurons and synapses.

For hardware implementations of ANNs, including SNNs and DNNs, it is crucial to integrate synapses, neurons, and peripheral circuits into interconnected systems at large array scales. When these components are seamlessly integrated, the system closely emulates biological neural networks, replicating core functionalities such as learning, memory, and cognition. This complete integration is essential for achieving adaptive and efficient processing observed in the human brain for tasks like pattern recognition, decision-making, and sensory processing. Yooyeon Jo et al. reported a configuration for an SNN System by integrating synapses and neurons[51]. Figure 5a illustrates a schematic of a small-scale SNN system constructed on a breadboard using RRAM and passive components to mimic a human neural network. In this system, volatile RRAM functions as neurons that send and receive signals, while non-volatile RRAM acts as synapses that determine signal strength and transmission. Input signals charge capacitor C_1 in an RC circuit, and when a specific threshold is exceeded, the volatile RRAM switches on, transmitting the signal to the post-neuron via the synapse. Like the pre-neuron, the post-neuron activates and generates output signals when the RC circuit exceeds a specific threshold. To realistically emulate LIF behavior seen in human neural transmission, resistors were connected in parallel with capacitors. Additionally, diodes and amplifiers were placed between synapses and post-neurons to prevent reverse leakage and ensure sufficient signal transmission to the post-neuron. By observing the voltage at each node in response to a same input pulse, we show that the output spike frequency of a post-neuron depends on the synaptic conductance in Fig. 5b. Furthermore, the number of output spikes is influenced not only by synaptic conductance but also by RC delay ($R_s \times C_{mem}$) and input voltage pulse conditions configured on the breadboard. Therefore, finding optimal parameters is crucial for neuromorphic system applications. The proposed SNN system performed

simulations on the MNIST dataset using experimentally obtained data for neurons and synapses in a network architecture of $784 \times 100 \times 10$. Input data were converted into Poisson spike trains, and the firing rates of each neuron were adjusted based on pixel values. The simulation achieved an accuracy of 83.45%, which is comparable to the ideal accuracy of 90.65%. Ensuring adequate device performance is essential for successful neuromorphic system implementation.

Kaichen Zhu et al. presented a neuromorphic system hybrid-integrated with CMOS systems and 2D-based RRAM[52]. They demonstrated a single cell of a 1T1M array fabricated by transferring h-BN nanosheets via a CMOS back-end-of-line (BEOL) process in Fig. 5c. The resulting device exhibited improved electrical characteristics compared to passive memristor devices, making it suitable for neuromorphic system implementation[53]. Based on these properties, unsupervised learning simulations were performed using an SNN on the MNIST dataset, achieving an average accuracy of 90%. The proposed system's network architecture, as shown in Fig. 5d, consisted of 784 input neurons, 400 excitatory neurons, 400 inhibitory neurons, and 10 output neurons. Furthermore, Fig. 5e illustrates a proposed CMOS circuit for hardware implementation of electronic neurons, which was verified through SPICE simulations. The proposed system used a hybrid configuration, integrating 2D-material-based RRAM technology with CMOS technology in a 1T1R structure for synapses, while a CMOS circuit was proposed to emulate the LIF behavior of biological neurons. A differential pair was included in the circuit to compute negative weights, and vector-matrix multiplication (VMM) operations occurred simultaneously in the neuromorphic array. To determine differential pair inputs, an input selection circuit was placed at the beginning, while an inverter amplifier at the end ensured spike generation when the membrane potential of the output neuron exceeded a threshold. SPICE simulation results confirmed that the frequency of post-spike generation varied depending on pre-spike timing as weights were adjusted according to the STDP learning rule in the SNN. The amount by which the membrane potential increases from the same input spike is changed according to the weight. The operation of the inverter amplifier demonstrated the Fire behavior of LIF by generating a post-spike when the voltage at a specific node exceeds the threshold. This study highlights the importance of integrating synaptic devices into large-scale
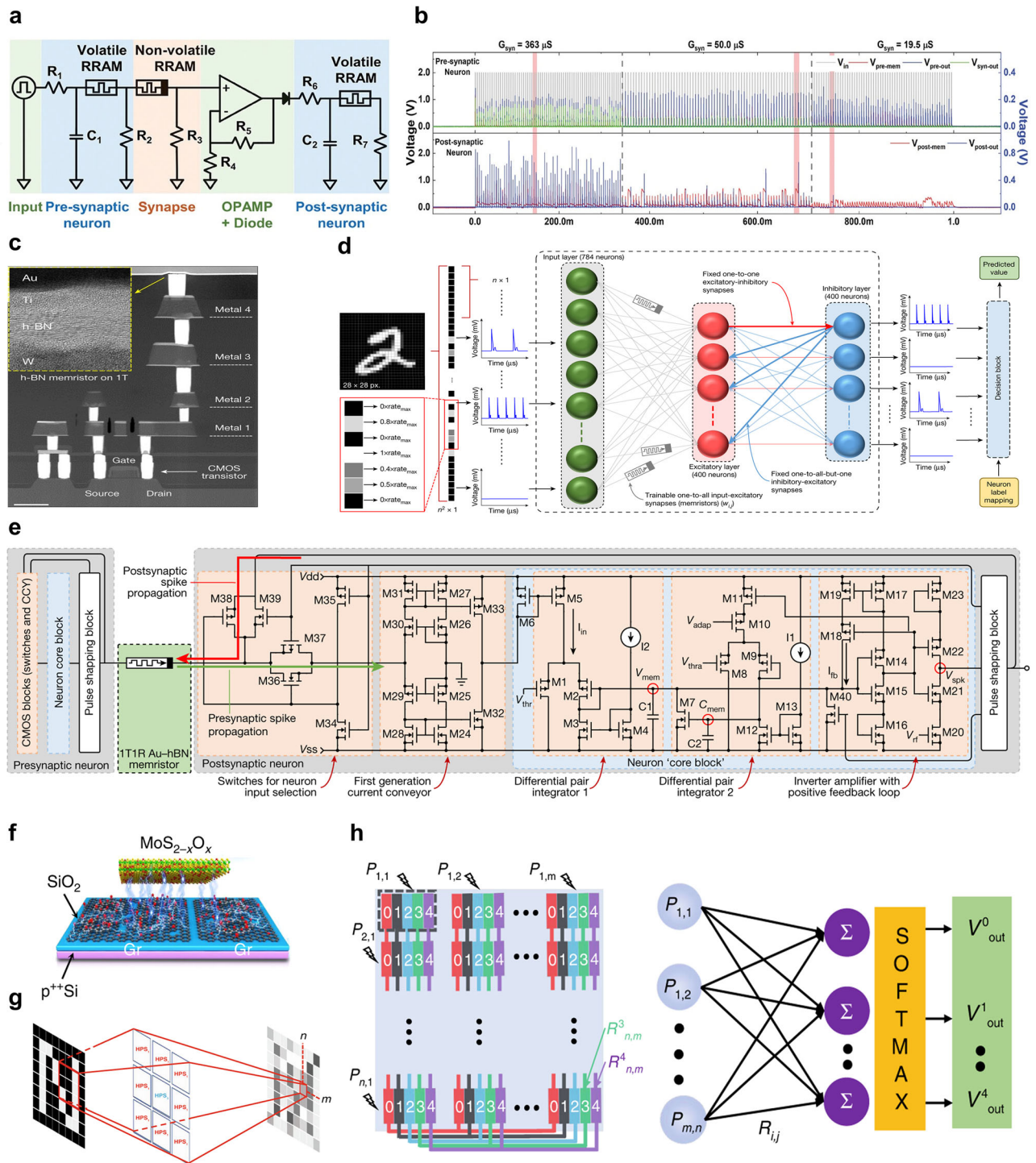
Fig. 5 | Neuromorphic System implementation. a Schematic design of circuit diagram[51]. **b** Transient electrical measurement of the ANN with three different conductance of the synaptic device. **c** cross-sectional scanning transmission electron microscope image of a 1T1M cell in the crossbar array[52]. **d** Structure of the considered SNN. Each MNIST image is reshaped as a 784 × 1 column vector, and the intensity of the pixels is encoded in terms of the firing frequency of the input neurons. The only trainable synapses are those connecting the input layer with the excitatory layer, and they are modeled with the STDP characteristic of the CMOS–h-BN based 1T1M cells.

e Circuit schematic of the proposed neuron–synapse–neuron block combining h-BN based 1T1M cells and CMOS circuitry. The colors indicate the complete neuron (gray surrounding box), the core block (light-blue box) and the individual building blocks (light-red boxes). **f** Schematic representation of the $MoS_{2-x}O_x$ structure with CVD-grown graphene electrodes[54]. **g** Feature extraction operation of opto-memristor sensor. **h** Schematic illustration of the single-layer perceptron photo memristors array for classifier emulation. Opto-memristors of the same class (color) are interconnected in parallel to generate the output current for the activation function.

arrays for neuromorphic system implementation. It also emphasizes that successful neuromorphic systems require not only improvements in the electrical characteristics of synapses but also concurrent research on neuron implementation.

Input considerations are also critical for practical neuromorphic system demonstrations. While most studies control inputs using semiconductor analyzers such as the B1500, edge computing applications could acquire inputs directly from sensors. Xiao Fu et al. reported an integrated sensor and

neuromorphic system using a nonvolatile opto-memristor array[54]. Figure 5f shows the structure of a non-volatile opto-memristor based on Graphene/$MoS_{2-x}O_x$/Graphene (Graphene/M/Graphene), used to mimic the human visual system. The human visual system performs two important roles: first, it organizes pre-processed images through feature extraction, and second, it classifies data obtained through the eyes. The preprocessing task is emulated by the CNN operation, and the opto-memristor array is used as a fixed kernel to extract the features of the input, as shown in Fig. 5g. This pre-processing reduces the computational complexity of subsequent operations by extracting features from analog images. Figure 5h also illustrates the classification functionality of the eye, implemented using a neural network. By pre-tuning the weights of the opto-memristor array, it acts as a single-layer perceptron with M×N inputs and 5 outputs. Consequently, the non-volatile opto-memristor array plays a key role in reducing latency between input and processing stages, mimicking the human visual system. In conclusion, although research on implementing large-scale neuromorphic systems based on 2D materials is still limited, research on small-scale systems is steadily progressing, paving the way for the implementation of true neuromorphic computing in the future.

Emerging applications of neuromorphic computing

Both 2D materials and neuromorphic computing have made significant advances in recent years. The combination of 2D materials like graphene with neuromorphic architectures brings unique advantages, such as enhanced conductivity, scalability, and the ability to mimic brain-like functionality through SNNs. These systems have the potential to revolutionize various fields by offering real-time adaptive learning, parallel processing, and significant energy efficiency. Applications span diverse domains, including autonomous systems, robotics, and healthcare, where neuromorphic systems can bridge the gap between human sensory capabilities and machine intelligence.

Neuromorphic systems in autonomous driving: enhancing vision

Neuromorphic vision systems are transforming autonomous technologies by addressing key challenges in real-time decision-making, adaptive navigation, and low-light imaging. Central to this transformation are photomemristors, which represent a significant advancement in neuromorphic vision by integrating sensing, memory, and computation into a single device.

In particular, VO_2-based photomemristors further extend the potential of neuromorphic systems by incorporating synaptic plasticity, a core feature of biological neural networks. Their unique phase transition properties allow for adaptive preprocessing, noise reduction, and enhanced object classification in UV-sensitive imaging scenarios. Li et al. showed that these devices improved image classification accuracy from 24% to 93%, illustrating their transformative impact on autonomous navigation and environmental monitoring[55]. These photomemristor technologies enable neuromorphic systems to achieve high-resolution imaging and adaptive decision-making, particularly in variable lighting conditions such as urban nightscapes and rural highways. By integrating these advancements, photomemristors serve as critical components in intelligent autonomous vision systems.

Complementing photomemristors, spiking neurons constructed with 2D subthreshold transistors (2D-ST) have emerged as a pivotal innovation in neuromorphic vision, particularly for enhancing real-time obstacle detection in autonomous vehicles. These systems effectively process data from sensors and cameras, enabling vehicles to respond dynamically to changing road conditions, obstacles, and traffic. This capability is critical for ensuring both energy efficiency and safety in self-driving cars, where rapid decision-making is essential. Thakar et al. demonstrated that 2D-ST neurons mimic the behavior of biological neurons, such as the lobula giant movement detector (LGMD) found in locusts, which specialize in detecting looming objects (Fig. 6a)[56]. The biomimetic design allows the system to register spikes efficiently as stimulus intensity increases, which mirrors the natural neural response to approaching objects (Fig. 6b). These spikes

increase in frequency as objects approach, peaking just before potential collision, ensuring a fast response time crucial for navigation (Fig. 6c). Moreover, the 2D-ST system exhibits exceptional energy efficiency, consuming as little as 3.5 pJ per spike for obstacle detection in real-time scenarios, and less than 100 pJ per detection event overall. Such efficiency, combined with rapid response times, makes it an ideal solution for energy-constrained applications like autonomous vehicles. Additionally, as shown in Fig. 6d, the system generates more spikes for inputs representing higher threat levels. For receding stimuli, it maintains efficient spike activity and reduces energy usage, which demonstrates its adaptability to varying environmental conditions (Fig. 6e-g). This precisely synchronized biomimetic approach facilitates seamless interaction between neuromorphic cores and external components. By utilizing real-time spike sensor data, these systems enhance autonomous vehicles' ability to detect collisions and respond rapidly to dynamic challenges.

Low-light traffic sensing, a persistent challenge for autonomous systems, has been significantly advanced through the integration of $MAPbI_3$/Bi_2O_2Se heterostructures into neuromorphic vision architectures (Fig. 6h, i)[57]. These materials exhibit exceptional photoresponsivity, surpassing 10^3 A/W under low-light conditions (Fig. 6j). This capability allows them to capture detailed visual information even in dim environments. Their high detectivity, exceeding 10^{12} Jones, ensures the accurate identification of subtle visual features, while their rapid photoelectric response times (less than 50 ms) minimize latency during visual processing. These heterostructures operate synergistically within neuromorphic frameworks, where their multi-state optoelectronic properties enable on-device memory and adaptive processing of visual inputs. For instance, their ability to encode light intensity into variable resistance states mimics the dynamic synaptic behavior of biological neural networks, facilitating real-time learning and decision-making. Additionally, the heterostructures' broad spectral sensitivity, from visible to near-infrared, enhances adaptability in diverse environments, such as detecting pedestrians in poorly lit urban areas or identifying obstacles in adverse weather conditions. Integrated into neuromorphic systems, their in-sensor computing capabilities reduce data transfer overhead, enabling low-power, high-speed image analysis directly within the device. This integration is pivotal for autonomous systems requiring energy-efficient operation, as it significantly reduces the reliance on external processors while maintaining high accuracy and responsiveness.

By integrating photomemristors, spiking neurons, and advanced heterostructures, neuromorphic vision systems are redefining the possibilities for autonomous navigation. These technologies collectively enhance energy efficiency, scalability, and adaptability, paving the way for safer and more efficient autonomous vehicles. Their critical role in bridging the gap between human-like perception and machine intelligence underscores the transformative impact of 2D materials in the field of neuromorphic vision.

Neuromorphic robotics systems: advancing interaction with 2D materials

2D materials have emerged as transformative components in neuromorphic tactile systems, particularly in robotics applications where precise interaction with dynamic environments is essential. By combining the ability to detect pressure, temperature, and texture with advanced computational features, 2D material-based devices address critical challenges such as scalability, efficiency, and adaptability in robotic systems, prosthetics, and wearable technologies. For instance, MoS_2-based electronic skin systems exemplify this innovation by integrating multimodal tactile sensing into a unified platform (Fig. 7a)[58]. These sensors detect pressure with a sensitivity of 0.5 kPa^{-1} in the low-pressure regime (< 100 kPa) and respond within 20 ms, providing the real-time feedback necessary for adaptive robotic manipulation. Additionally, the system demonstrated nociceptive behavior, as shown in Fig. 7b, where the output current increases with both rising pulse amplitudes (0.6 V to 1.2 V) and varying pulse widths (10 μs to 2 ms). Moreover, they simultaneously measure strain and temperature variations, processing these signals to emulate the comprehensive sensory feedback mechanisms of human skin (Fig. 7c). Such capabilities allow robots to
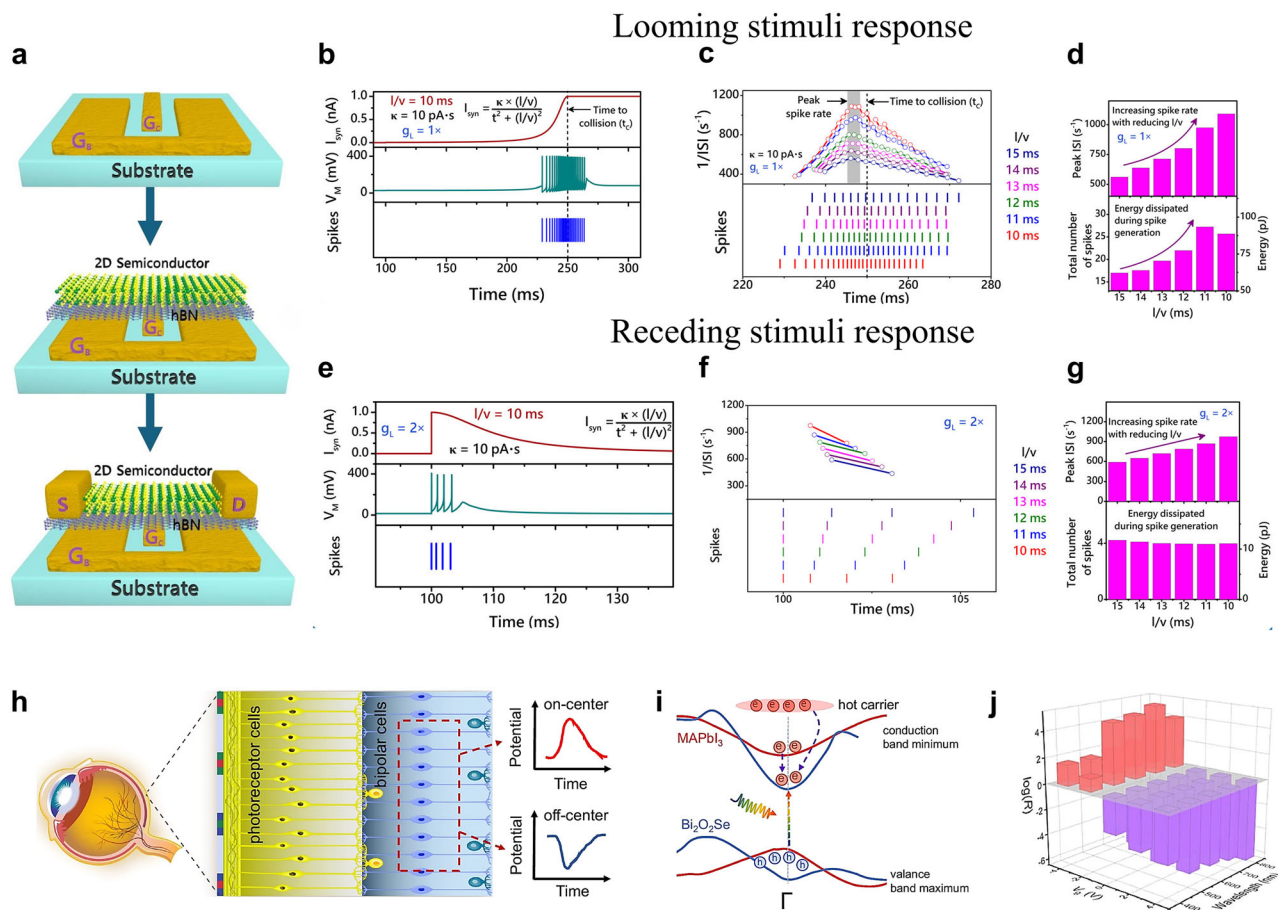
Fig. 6 | Neuromorphic systems in autonomous driving. a Schematic of the fabrication process for a 2D-ST with a multi-gate structure[56]. b Circuit response (VM and raster plot) for an Isyn pulse (100–250 ms), simulating synaptic input into an LGMD neuron for a looming stimulus. c Graph showing the instantaneous spike rate (top) and spike timing (bottom) for various I/v inputs. d As I/v decreases, peak interspike interval (ISI) and the total number of spikes (and energy) increase, suggesting that higher-threat inputs prompt a more intense response but at the cost of greater energy consumption. e–g Similar data as (e-g) but for receding stimuli, showing an increased leakage conductance (gL). h Schematic of the human retina's photoreceptor and bipolar cell structure for low-light traffic sensing[57]. i Interband photoexcitation and hot-carrier transition in the MAPbI$_3$/Bi$_2$O$_2$Se heterostructure. j Enhanced photoresponsivity (exceeding 10^3 A/W) of MAPbI$_3$/Bi$_2$O$_2$Se heterostructures across the visible spectrum (400–800 nm), enabling low-light imaging.

perform complex tasks like handling delicate objects or navigating uncertain terrains with greater precision and adaptability.

In addition to enhancing tactile sensing, 2D materials play a pivotal role in advancing neuromorphic functionalities for robotics. Quin et al. introduced SnSe-based TSMs as advanced devices that seamlessly integrate sensory detection with memory and computation (Fig. 7d)[59]. Operating with volatile resistance switching, the TSM achieves a low threshold voltage (< 0.6 V) and an ON-OFF ratio of 10^4, enabling precise encoding and processing of tactile inputs. Beyond their sensory capabilities, the computational properties of SnSe-based TSMs significantly enhance their utility. Their stochastic behavior facilitates integration into neuromorphic computing architectures, particularly in constructing stochastic LIF neuron models (Fig. 7e, f). These models are essential for implementing energy-efficient neuromorphic systems capable of real-time decision-making. When tested on the MNIST dataset, the TSM-based architecture demonstrated a classification accuracy of 93% (Fig. 7g). This dual capability of combining tactile sensing with neuromorphic computation provides a streamlined approach to tactile data processing, empowering robots to dynamically adapt to varying environmental conditions.

The integration of neuromorphic systems into robotics is further advanced by multisensory devices capable of cross-modal perception. Inspired by the biological principles of multisensory integration, such as those observed in macaques' ocular-vestibular systems, bioinspired motion-

cognition systems emulate the ability to combine visual and inertial cues for enhanced spatial awareness. Jiang et al. showed the use of dual-gate flexible synaptic transistors fabricated from 2D-nanoflake thin films (Fig. 7h)[60]. These devices exhibit spatiotemporal integration and history-dependent plasticity, which allow them to process multimodal sensory inputs in a parallel and event-driven manner. In practical demonstrations, bimodal signals from an accelerometer and gyroscope were encoded as spatiotemporal spike trains. This enabled the synaptic transistor to differentiate motion types such as human activities and drone flight modes. The neuromorphic system demonstrated high classification accuracy, with a 94% success rate in human activity recognition and 95% in drone flight mode recognition (Fig. 7i). By leveraging presynaptic and postsynaptic signal outputs, the system surpasses traditional sensory-processing units in energy efficiency and accuracy.

The integration of 2D materials and neuromorphic systems provides significant advancements in robotics, addressing key challenges in precision, adaptability, and energy efficiency. By combining tactile sensing, memory, and computation, these technologies enable robots to perform real-time decision-making in dynamic environments. Applications range from emulating biological sensory mechanisms to implementing multisensory integration, supporting improved functionality in industrial automation. These developments establish 2D material-based neuromorphic systems as critical components for the next generation of intelligent robotics.
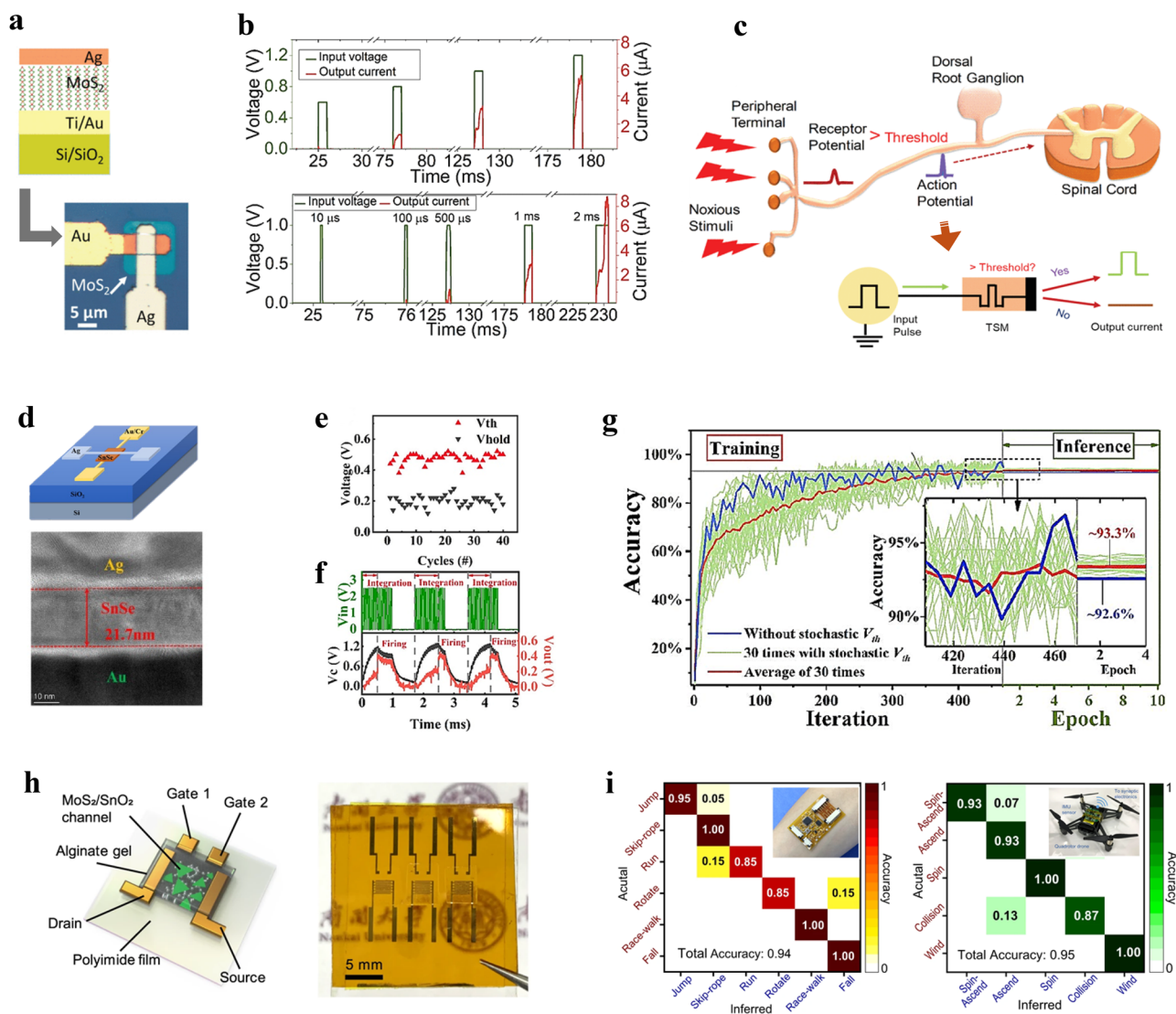
Fig. 7 | Neuromorphic robotics systems. a Schematic illustration of the Au/MoS$_2$/Ag threshold switching memristors (TSM) device (top) and an optical image of the fabricated device (bottom)[58]. b Output current of the artificial nociceptor for increasing pulse amplitudes (0.6 V to 1.2 V) at a fixed pulse width of 1 ms (top) and output current of the artificial nociceptor for varying pulse widths (10 μs to 2 ms) at a constant pulse amplitude of 1 V (bottom). c Schematic of biological nociceptor and its key features (top) and block diagram illustrating the architecture of the MoS$_2$ TFT-based artificial noc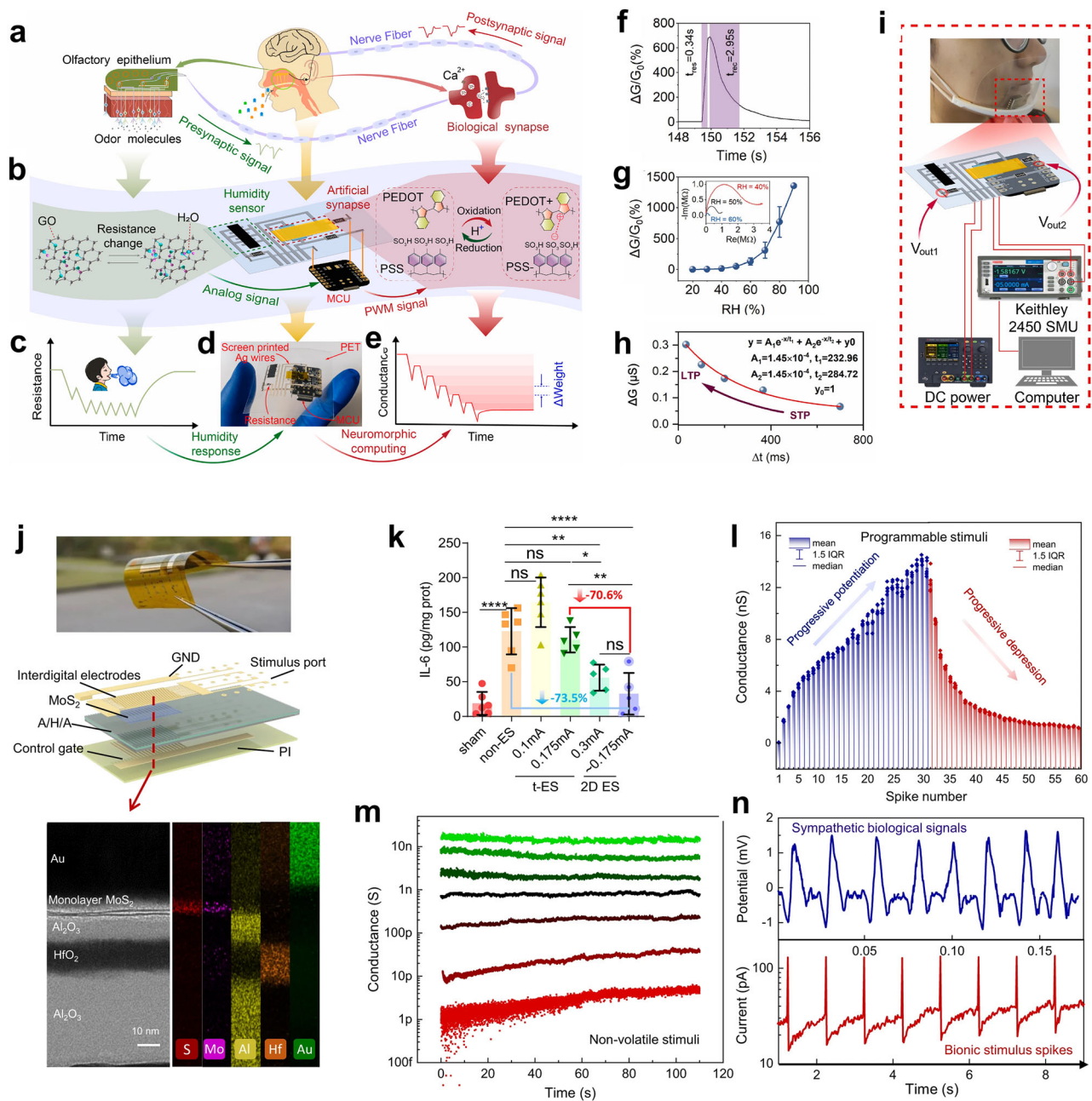iceptor (bottom). d Schematic illustration of the Ag/SnSe/Au TS device (top) and cross-sectional HRTEM image of the device (bottom)[59]. e Temporal evolution of the membrane potential (black) of a LIF neuron in response to a series of input spikes (green). The neuron fires when the membrane potential exceeds the threshold, generating an output spike (red). f Stochastic LIF neuron operation. g Classification accuracy of the TSM-based neural network on the MNIST dataset. h Schematic and optical image of the flexible dual-gate synaptic transistor[60]. i Confusion matrices for human activity recognition (left) and drone flight mode classification (right) using SNN.

Neuromorphic systems in healthcare: from real-time monitoring to active intervention

Neuromorphic systems integrated with advanced 2D materials offer transformative potential in healthcare applications, particularly in enhancing real-time monitoring and adaptive responses. By leveraging the unique properties of 2D materials, these systems provide innovative solutions for tracking vital signs, detecting abnormalities, and enabling early interventions. Zhao et al. developed an artificial respiratory perception system integrating sensing, memory, and computing functionalities on a single polymer substrate[61]. At the heart of this system is a graphene oxide (GO)-based humidity sensor, which binds exhaled water molecules using its large surface area and oxygen-containing functional groups. These interactions produce measurable resistance changes, converted into pulse-width modulation (PWM) signals by a microcontroller unit (MCU). The signals are then processed by an organic electrochemical artificial synapse (OEAS), which adjusts its conductance based on respiratory patterns (Fig. 8a–e). The

GO sensor demonstrates rapid response (0.34 s), efficient recovery (2.95 s at 77% relative humidity; Fig. 8f), and high sensitivity (0.041; Fig. 8g) enabling precise real-time tracking of respiratory variations. The OEAS component enhances neuromorphic functionality with over 100 conductance states, mimicking short-term and long-term plasticity to differentiate subtle respiratory behavior changes (Fig. 8h). This allows for the accurate detection of abnormalities, such as variations in breathing intensity as small as 5%, which could indicate early signs of respiratory disorders. Furthermore, this integrated system eliminates the need for external computational resources, resulting in a compact and energy-efficient design suitable for wearable healthcare applications (Fig. 8i). These advancements underline the critical role of neuromorphic systems in healthcare, offering innovative solutions for real-time monitoring, early diagnosis, and personalized treatment.

In addition to health monitoring, neuromorphic electrostimulation devices based on 2D materials show potential for applications in inflammation management. MoS$_2$-based FGM devices exemplify this approach,

Fig. 8 | Neuromorphic Systems in Healthcare. a Schematic illustration of the artificial respiratory perception system, integrating a GO humidity sensor and an OEAS[61]. **b** Optical image of the flexible GO humidity sensor. **c** Response and recovery characteristics of the GO humidity sensor. **d** System architecture, showing the integration of the GO sensor with the OEAS and MCU. **e** Conductance modulation of the OEAS under various input pulse conditions. **f** The response and recovery times of GO humidity sensor at 77% RH. **g** The GO humidity sensor exhibits increased sensitivity to increasing humidity levels (20–90% RH). The sensor exhibits a strong logarithmic relationship between resistance and relative humidity, with a sensitivity (i.e., slope) of 0.041. **h** The device's conductance increases with pulse frequency and duration. Repeated pulses can induce a long-term memory state, with shorter pulse intervals accelerating this process. **i** Demonstration of the system integrated into a face mask for real-time respiratory monitoring. **j** Schematic illustration of the MoS$_2$-based floating-gate memory (FGM) device (top) and its integration into a neuromorphic stimulation system (bottom)[39]. **k** 2D-based neuromorphic stimulation reduced IL-6 levels by 73.5% compared to traditional electrical stimulation, while using significantly lower current levels (41.7% less). **l** The device exhibits synaptic plasticity, with its conductance increasing or decreasing based on the applied stimulus, mimicking the long-term potentiation and long-term depression processes observed in biological synapses. **m** Enabling the programming of specific conductance states, mimicking the long-term potentiation and long-term depression observed in biological synapses. This allows for the delivery of precise and personalized stimulation patterns. **n** Recorded sympathetic nerve signals (top) and the delivered neuromorphic stimulation pulses (bottom).

utilizing programmable bionic spikes to achieve minimally invasive nerve stimulation (Fig. 8j)[39]. Unlike conventional electrical stimulation techniques, which risk nerve damage due to high currents, these neuromorphic systems enable ultra-low current operation (as low as 0.175 mA) while effectively reducing inflammatory responses. For instance, the modulation of sympathetic nerve activity using such devices has been shown to decrease

cytokine IL-6 levels by 73.5%, highlighting their efficacy in treating inflammatory diseases (Fig. 8k). The programmable nature of these neuromorphic devices allows for real-time adaptation, mimicking synaptic plasticity to deliver tailored stimulation patterns based on patient-specific conditions (Fig. 8l–n). This feature is particularly valuable in clinical settings for managing chronic inflammation or facilitating recovery from tendon

injuries, where traditional treatments often face limitations. Furthermore, the biocompatible properties of 2D materials, such as minimal cytotoxicity, make them suitable for long-term implantation, ensuring both safety and effectiveness in medical applications.

These innovations underscore the expanding role of neuromorphic systems in healthcare, moving beyond monitoring to active intervention. By integrating sensing, processing, and therapeutic functions, 2D material-based neuromorphic technologies offer a unified platform for addressing complex medical challenges.

Outlook

The integration of 2D materials for AI hardware holds immense potential, presenting both significant opportunities and challenges for future research.

First, the unique electrical properties of 2D materials, combined with their scalability and mechanical flexibility[44,62,63], open up new possibilities for use in flexible and wearable electronics and optoelectronics, particularly in areas such as biomedical devices and soft robotics[64]. These materials can maintain high performance even under deformation and are excellent building blocks to realize heterogeneous structures, further enhancing their potential in the development of more complex neuromorphic systems.

Thanks to these prominent characteristics, 2D materials have showcased excellent resistive switching capabilities even at the monolayer level, positioning them as a promising solution to overcome the vertical scaling limitations of traditional 3D material-based memristors[65,66]. The integration of 2D memristors into 3D architectures enables ultra-high-density memory arrays and highly efficient neuromorphic systems, leading to substantial advancements in parallel processing and computational efficiency[67–69]. By stacking various 2D materials[12,15,70–76], enhanced synaptic functions such as multi-state switching and tunable plasticity can be achieved, both of which are crucial for implementing more advanced neuromorphic architectures. Furthermore, their fast-switching speeds and low-power operation have made them highly attractive for next-generation neuromorphic devices, superior to the slow switching speeds of commercialized 3D material-based memristors that has approximately slower than conventional DRAM.

Despite remarkable progress, several key challenges must be overcome as well. One of the primary obstacles is the scalability and uniformity of 2D materials applied in neuromorphic devices[77,78]. Albeit several advancements in 2D synthesis techniques[79,80], producing large-area, defect-free 2D materials remains a major hurdle[19,36,81], which is essential for their future commercialization in industries for flexible electronics and quantum computing[18,19,82,83]. AI can also play a crucial role in this context by optimizing synthesis processes and predicting the best conditions for material growth, thus improving the quality and scalability of these materials.

Another significant challenge is integrating 2D materials into existing technologies. As device structures become more complex, it is vital to seamlessly integrate 2D materials into current manufacturing processes, ensure compatibility with silicon-based technologies, and develop new methods for multi-layered architectures[84]. Additionally, the environmental stability of 2D materials remains a concern, as many of them are sensitive to humidity, temperature, and oxidation. Future research must focus on developing protective coatings or hybrid materials that can maintain the advantageous properties of 2D materials while enhancing their durability. AI can aid in discovering these protective strategies by rapidly screening potential compounds and predicting their effectiveness.

In conclusion, despite that oxide-based memristor devices are still widely used in neuromorphic computing, ongoing research on 2D materials presents promising alternatives. As processing technologies for 2D materials continue to advance, they may not only compete with oxide-based memristors in terms of performance, but also offer unique advantages in high flexibility, scalability, and innovative features. These developments could be expected to revolutionize the design and implementation of next-generation neuromorphic systems toward more energy-efficient, large-scale, and flexible computing architectures.

References

1. Li, X. et al. Power-efficient neural network with artificial dendrites. *Nature Nanotechnology* **15**, 776–782 (2020).
2. Pei, J. et al. Towards artificial general intelligence with hybrid Tianjic chip architecture. *Nature* **572**, 106–111 (2019).
3. Zhang, W. et al. Neuro-inspired computing chips. *Nature electronics* **3**, 371–382 (2020).
4. Kendall, J. D. & Kumar, S. The building blocks of a brain-inspired computer. *Applied Physics Reviews* **7** (2020).
5. Moore, G. E. Cramming more components onto integrated circuits. *Proceedings of the IEEE* **86**, 82–85 (1998).
6. Berl, A. et al. Energy-efficient cloud computing. *The computer journal* **53**, 1045–1051 (2010).
7. Lee, Y. C. & Zomaya, A. Y. Energy efficient utilization of resources in cloud computing systems. *The Journal of Supercomputing* **60**, 268–280 (2012).
8. Mukherjee, T., Banerjee, A., Varsamopoulos, G., Gupta, S. K. & Rungta, S. Spatio-temporal thermal-aware job scheduling to minimize energy consumption in virtualized heterogeneous data centers. *Computer Networks* **53**, 2888–2904 (2009).
9. Zou, X., Xu, S., Chen, X., Yan, L. & Han, Y. Breaking the von Neumann bottleneck: architecture-level processing-in-memory technology. *Science China Information Sciences* **64**, 160404 (2021).
10. Cai, F. et al. A fully integrated reprogrammable memristor–CMOS system for efficient multiply–accumulate operations. *Nature electronics* **2**, 290–299 (2019).
11. Yang, J. T. et al. Artificial synapses emulated by an electrolyte-gated tungsten-oxide transistor. *Advanced Materials* **30**, 1801548 (2018).
12. Geim, A. K. & Grigorieva, I. V. Van der Waals heterostructures. *Nature* **499**, 419–425 (2013).
13. Liu, Y., Huang, Y. & Duan, X. Van der Waals integration before and beyond two-dimensional materials. *Nature* **567**, 323–333 (2019).
14. Novoselov, K. S., Mishchenko, A., Carvalho, A. & Castro Neto, A. 2D materials and van der Waals heterostructures. *Science* **353**, aac9439 (2016).
15. Meng, Y. et al. Photonic van der Waals integration from 2D materials to 3D nanomembranes. *Nature Reviews Materials* **8**, 498–517 (2023).
16. Meng, Y. et al. Functionalizing nanophotonic structures with 2D van der Waals materials. *Nanoscale Horizons* **8**, 1345–1365 (2023).
17. Kang, J.-H. et al. Monolithic 3D integration of 2D materials-based electronics towards ultimate edge computing solutions. *Nature Materials* **22**, 1470–1477 (2023).
18. Jiang, J. & Su, J. in *2D Materials for Electronics, Sensors and Devices* 259-285 (Elsevier, 2023).
19. Xia, X. et al. 2D-material-based volatile and nonvolatile memristive devices for neuromorphic computing. *ACS Materials Letters* **5**, 1109–1135 (2023).
20. Sangwan, V. K. et al. Multi-terminal memtransistors from polycrystalline monolayer molybdenum disulfide. *Nature* **554**, 500–504 (2018).
21. Zhu, X., Li, D., Liang, X. & Lu, W. D. Ionic modulation and ionic coupling effects in MoS2 devices for neuromorphic computing. *Nature materials* **18**, 141–148 (2019).
22. Wu, X., Dang, B., Zhang, T., Wu, X. & Yang, Y. Spatiotemporal audio feature extraction with dynamic memristor-based time-surface neurons. *Science Advances* **10**, eadl2767 (2024).
23. Feng, X. et al. Self-selective multi-terminal memtransistor crossbar array for in-memory computing. *ACS nano* **15**, 1764–1774 (2021).

24. Shen, Z. et al. Advances of RRAM devices: Resistive switching mechanisms, materials and bionic synaptic application. *Nanomaterials* **10**, 1437 (2020).

25. Wang, S. et al. Physically transient diode with ultrathin tunneling layer as selector for bipolar one diode-one resistor memory. *IEEE Electron Device Letters* **42**, 700–703 (2021).

26. Ji, X., Hao, S., Pang, K. Y., Lim, K. G. & Zhao, R. A vacuum gap selector with ultra-low leakage for large-scale neuromorphic network. *IEEE Electron Device Letters* **41**, 505–508 (2020).

27. Wang, Z. et al. Resistive switching materials for information processing. *Nature Reviews Materials* **5**, 173–195 (2020).

28. Gerasimov, J. Y. et al. An evolvable organic electrochemical transistor for neuromorphic applications. *Advanced Science* **6**, 1801339 (2019).

29. Sun, W. et al. Understanding memristive switching via in situ characterization and device modeling. *Nature communications* **10**, 3453 (2019).

30. Zhao, M., Li, R. & Xue, J. Atomic bridge memristor based on silver and two-dimensional GeSe. *AIP advances* **10** (2020).

31. Teja Nibhanupudi, S. et al. Ultra-fast switching memristors based on two-dimensional materials. *Nature Communications* **15**, 2334 (2024).

32. Hirose, Y. & Hirose, H. Polarity-dependent memory switching and behavior of Ag dendrite in Ag-photodoped amorphous As2S3 films. *Journal of Applied Physics* **47**, 2767–2772 (1976).

33. Pan, L. et al. Metal-organic framework nanofilm for mechanically flexible information storage applications. *Advanced Functional Materials* **25**, 2677–2685 (2015).

34. Kwon, D.-H. et al. Atomic structure of conducting nanofilaments in TiO2 resistive switching memory. *Nature nanotechnology* **5**, 148–153 (2010).

35. Li, D. et al. MoS2 memristors exhibiting variable switching characteristics toward biorealistic synaptic emulation. *ACS nano* **12**, 9240–9252 (2018).

36. Naqi, M. et al. Multilevel artificial electronic synaptic device of direct grown robust MoS2 based memristor array for in-memory deep neural network. *npj 2D Materials and Applications* **6**, 53 (2022).

37. Rasouli, H. R. et al. Electric-field-induced reversible phase transitions in a spontaneously ion-intercalated 2D metal oxide. *Nano Letters* **21**, 3997–4005 (2021).

38. Pal, A. et al. An ultra energy-efficient hardware platform for neuromorphic computing enabled by 2D-TMD tunnel-FETs. *Nature Communications* **15**, 3392 (2024).

39. Bao, R. et al. Neuromorphic electro-stimulation based on atomically thin semiconductor for damage-free inflammation inhibition. *Nature Communications* **15**, 1327 (2024).

40. Bae, J., Won, J. & Shim, W. The rise of memtransistors for neuromorphic hardware and In-memory computing. *Nano Energy*, 109646 (2024).

41. Ding, G. et al. Reconfigurable 2D WSe2-based memtransistor for mimicking homosynaptic and heterosynaptic plasticity. *Small* **17**, 2103175 (2021).

42. Huang, X. et al. An ultrafast bipolar flash memory for self-activated in-memory computing. *Nature nanotechnology* **18**, 486–492 (2023).

43. Guo, L. Q. et al. Oxide neuromorphic transistors gated by polyvinyl alcohol solid electrolytes with ultralow power consumption. *ACS applied materials & interfaces* **11**, 28352–28358 (2019).

44. Kim, S. H. et al. Electrolyte-gated transistors for organic and printed electronics. *Advanced Materials* **25**, 1822–1846 (2013).

45. Shu, H. et al. Dynamic model of the short-term synaptic behaviors of PEDOT-based organic electrochemical transistors with modified Shockley equations. *ACS omega* **7**, 14622–14629 (2022).

46. Yan, Y. et al. High-performance organic electrochemical transistors with nanoscale channel length and their application to artificial synapse. *ACS Applied Materials & Interfaces* **12**, 49915–49925 (2020).

47. Liao, J. et al. Van der Waals ferroelectric semiconductor field effect transistor for in-memory computing. *ACS nano* **17**, 6095–6102 (2023).

48. Han, S. et al. High energy density in artificial heterostructures through relaxation time modulation. *Science* **384**, 312–317 (2024).

49. Zagni, N., Pavan, P. & Alam, M. A. A memory window expression to evaluate the endurance of ferroelectric FETs. *Applied Physics Letters* **117** (2020).

50. Jeong, Y. et al. Engineering MoSe2/MoS2 heterojunction traps in 2D transistors for multilevel memory, multiscale display, and synaptic functions. *npj 2D Materials and Applications* **6**, 23 (2022).

51. Jo, Y. et al. Hardware implementation of network connectivity relationships using 2D hBN-based artificial neuron and synaptic devices. *Advanced Functional Materials* **34**, 2309058 (2024).

52. Zhu, K. et al. Hybrid 2D–CMOS microchips for memristive applications. *Nature* **618**, 57–62 (2023).

53. Kim, M. et al. Analogue switches made from boron nitride monolayers for application in 5G and terahertz communication systems. *Nature Electronics* **3**, 479–485 (2020).

54. Fu, X. et al. Graphene/MoS2− xOx/graphene photomemristor with tunable non-volatile responsivities for neuromorphic vision processing. *Light: Science & Applications* **12**, 39 (2023).

55. Li, G. et al. Photo-induced non-volatile VO2 phase transition for neuromorphic ultraviolet sensors. *Nature communications* **13**, 1729 (2022).

56. Thakar, K., Rajendran, B. & Lodha, S. Ultra-low power neuromorphic obstacle detection using a two-dimensional materials-based subthreshold transistor. *npj 2D Materials and Applications* **7**, 68 (2023).

57. Xu, L. et al. Ultrasensitive dim-light neuromorphic vision sensing via momentum-conserved reconfigurable van der Waals heterostructure. *Nature Communications* **15**, 9011 (2024).

58. Dev, D., Shawkat, M. S., Krishnaprasad, A., Jung, Y. & Roy, T. Artificial nociceptor using 2D MoS 2 threshold switching memristor. *IEEE Electron Device Letters* **41**, 1440–1443 (2020).

59. Qin, Y. et al. Threshold switching memristor based on 2D SnSe for nociceptive and leaky-integrate and fire neuron simulation. *ACS Applied Electronic Materials* **6**, 4939–4947 (2024).

60. Jiang, C. et al. Mammalian-brain-inspired neuromorphic motion-cognition nerve achieves cross-modal perceptual enhancement. *Nature Communications* **14**, 1344 (2023).

61. Zhao, Q.-L. et al. Olfactory-inspired neuromorphic artificial respiratory perception system with graphene oxide humidity sensor and organic electrochemical transistor. *Carbon* **218**, 118765 (2024).

62. Bae, S.-H. et al. Integration of bulk materials with two-dimensional materials for physical coupling and applications. *Nature Materials* **18**, 550–560 (2019).

63. Hou, W. et al. Strain engineering of vertical molybdenum ditelluride phase-change memristors. *Nature Electronics* **7**, 8–16 (2024).

64. Li, Z. et al. Crossmodal sensory neurons based on high-performance flexible memristors for human-machine in-sensor computing system. *Nature Communications* **15**, 7275 (2024).

65. Kim, K., Choi, J.-Y., Kim, T., Cho, S.-H. & Chung, H.-J. J. N. A role for graphene in silicon-based semiconductor devices. *Nature* **479**, 338–344 (2011).

66. Song, M.-K. et al. Recent Advances and Future Prospects for Memristive Materials, Devices, and Systems. *ACS Nano* **17**, 11994–12039 (2023).

67. Shulaker, M. M. et al. Three-dimensional integration of nanotechnologies for computing and data storage on a single chip. *Nature* **547**, 74–78 (2017).

68. Shin, J. et al. Vertical full-colour micro-LEDs via 2D materials-based layer transfer. *Nature* **614**, 81–87 (2023).

69. Choi, C. et al. Reconfigurable heterogeneous integration using stackable chips with embedded artificial intelligence. *Nature Electronics* **5**, 386–393 (2022).

70. Castellanos-Gomez, A. et al. Van der Waals heterostructures. *Nature Reviews Methods Primers* **2**, 58 (2022).

71. Hou, H. L., Anichini, C., Samorì, P., Criado, A. & Prato, M. 2D Van der Waals heterostructures for chemical sensing. *Advanced Functional Materials* **32**, 2207065 (2022).

72. Meng, Y. et al. Ultracompact graphene-assisted tunable waveguide couplers with high directivity and mode selectivity. *Scientific Reports* **8**, 1–11 (2018).

73. Tan, S. H. et al. Perspective: Uniform switching of artificial synapses for large-scale neuromorphic arrays. *APL Materials* **6** (2018).

74. Zhao, T. et al. Ultrathin MXene assemblies approach the intrinsic absorption limit in the 0.5–10 THz band. *Nature Photonics* **17**, 622–628 (2023).

75. He, T. et al. Optical skyrmions from metafibers with subwavelength features. *Nature Communications* **15**, 10141 (2024).

76. Tang, B. et al. Wafer-scale solution-processed 2D material analog resistive memory array for memory-based computing. *Nature Communications* **13**, 3037 (2022).

77. He, T. et al. On-chip optoelectronic logic gates operating in the telecom band. *Nature Photonics* **18**, 60–67 (2024).

78. Meng, Y. et al. Waveguide engineering of graphene optoelectronics—modulators and polarizers. *IEEE Photonics Journal* **10**, 1–17 (2018).

79. Solís-Fernández, P., Bissett, M. & Ago, H. Synthesis, structure and applications of graphene-based 2D heterostructures. *Chemical Society Reviews* **46**, 4572–4613 (2017).

80. Choi, S. H. et al. Large-scale synthesis of graphene and other 2D materials towards industrialization. *Nature Communications* **13**, 1484 (2022).

81. Kim, K. S. et al. Non-epitaxial single-crystal 2D material growth by geometric confinement. *Nature* **614**, 88–94 (2023).

82. Guo, Q. et al. Ultrathin quantum light source with van der Waals NbOCl2 crystal. *Nature* **613**, 53–59 (2023).

83. Turunen, M. et al. Quantum photonics with layered 2D materials. *Nature Reviews Physics* **4**, 219–236 (2022).

84. Akinwande, D. et al. Graphene and two-dimensional materials for silicon technology. *Nature* **573**, 507–518 (2019).

85. Wang, K. et al. A pure 2H-MoS2 nanosheet-based memristor with low power consumption and linear multilevel storage for artificial synapse emulator. *Advanced Electronic Materials* **6**, 1901342 (2020).

86. Lian, X. et al. Electrical properties and biological synaptic simulation of Ag/MXene/SiO2/Pt RRAM devices. *Electronics* **9**, 2098 (2020).

87. He, N. et al. V_2C-based memristor for applications of low power electronic synapse. *IEEE Electron Device Letters* **42**, 319–322 (2021).

88. Farronato, M. et al. Memtransistor devices based on MoS2 multilayers with volatile switching due to Ag cation migration. *Advanced Electronic Materials* **8**, 2101161 (2022).

89. Peng, Z. et al. Flexible memristor constructed by 2D cadmium phosphorus trichalcogenide for artificial synapse and logic operation. *Advanced Functional Materials* **33**, 2211269 (2023).

90. Yan, X. et al. Memristors based on multilayer graphene electrodes for implementing a low-power neuromorphic electronic synapse. *Journal of Materials Chemistry C* **8**, 4926–4933 (2020).

91. Zhou, Z. et al. Designing carbon conductive filament memristor devices for memory and electronic synapse applications. *Materials Horizons* **7**, 1106–1114 (2020).

92. Wu, X. et al. Thinnest nonvolatile memory based on monolayer h-BN. *Advanced Materials* **31**, 1806790 (2019).

93. Fatima, S., Tahir, R., Akinwande, D. & Rizwan, S. Enhanced memristive effect of laser-reduced graphene and ferroelectric MXene-based flexible trilayer memristors. *Carbon* **218**, 118656 (2024).

94. Vu, Q. A. et al. Two-terminal floating-gate memory with van der Waals heterostructures for ultrahigh on/off ratio. *Nature communications* **7**, 12725 (2016).

95. Liu, C. et al. A semi-floating gate memory based on van der Waals heterostructures for quasi-non-volatile applications. *Nature nanotechnology* **13**, 404–410 (2018).

96. Zhang, X. et al. Programmable neuronal-synaptic transistors based on 2D MXene for a high-efficiency neuromorphic hardware network. *Matter* **5**, 3023–3040 (2022).

97. Sharbati, M. T. et al. Low-power, electrochemically tunable graphene synapses for neuromorphic computing. *Advanced Materials* **30**, 1802353 (2018).

98. Chen, Y. et al. Highly linear and symmetric synaptic memtransistors based on polarization switching in two-dimensional ferroelectric semiconductors. *Small* **18**, 2203611 (2022).

99. Liu, K. et al. An optoelectronic synapse based on α-In2Se3 with controllable temporal dynamics for multimode and multiscale reservoir computing. *Nature Electronics* **5**, 761–773 (2022).

100. Wang, S. et al. Two-dimensional ferroelectric channel transistors integrating ultra-fast memory and neural computing. *Nature Communications* **12**, 53 (2021).

Acknowledgements

Author contributions

Y.C., S.H., Z.X., Y.M. and S.X. were responsible for the conceptualization of the paper, data curation, illustrations, and writing of the Synaptic Devices Based on 2D Materials. H.J., S.E.Y., M.S., and J.-H.K. were responsible for data curation, illustrations, and writing of the Neuromorphic System Demonstration section. They contributed to the review and editing process, with J.-H.K. additionally providing supervision during the development of the section. S.J., J.K., M.S.C., and S.M. were responsible for the data curation, illustrations, and writing of the Emerging Applications of Neuromorphic Computing section. They participated in the review and editing process, with S.M. additionally providing supervision and project administration. S.H.B. was responsible for the conceptualization of the paper, funding acquisition, project administration, resources, and supervision. He also contributed to data curation, illustrations, and writing of this review paper, as well as the review and editing of the manuscript. All authors have read and approved the final manuscript.

Competing interests

The authors declare no competing interests.

Additional information

Correspondence and requests for materials should be addressed to Ji-Hoon Kang, Sungchul Mun or Sang-Hoon Bae.

Reprints and permissions information is available at http://www.nature.com/reprints